Microchimica Acta (2022) 189: 251
https://doi.org/10.1007/s00604-022-05348-9

ORIGINAL PAPER

Gold nanoparticle functionalized nanopipette sensors for electrochemical paraquat detection

Yazhou Xiong[1] · Tao Ma[1,2] · Hao Zhang[1] · Lizhu Qiu[1] · Shuai Chang[1] · Yingwei Yang[3] · Feng Liang[1,2]

Received: 9 November 2021 / Accepted: 15 May 2022 / Published online: 10 June 2022

Abstract

A sensitive nanopipette sensor is established through a unique design of host–guest recognition, which could be further enhanced by the introduction of gold nanoparticles (Au NPs). Generally, the nanopipette is conjugated with caboxylatopillar[5]arenes (CP[5]) or carboxylated leaning pillar[6]arene (CLP[6]) to generate recognition sites. After the addition of pesticide molecules, they would be captured by CP[5] (or CLP[6]), resulting in a significant electronegativity change on the nanopipette's inner surface, which could be determined by the ionic current change. The CP[5]-modified nanopipette exhibited reliable selectivity for paraquat, while the CLP[6]-modified nanopipette showed an ability of detection for both paraquat and diquat. The addition of Au NPs improved the selectivity and sensitivity of the CP[5]-Au NP-modified nanopipette for paraquat sensing. After optimization by lowering the size of the Au NPs, CP[5]-Au NPs (3 nm)-modified nanopipettes achieved lower detection limits of 0.034 nM for paraquat. Furthermore, in real sample analysis, this sensor demonstrates exceptional sensitivity and selectivity. This study provides a new strategy to develop nanopipette sensors for practical small molecule detection.

Keywords Nanopipette sensors · Pillararenes · Host–guest interaction · Gold nanoparticles · Paraquat

Introduction

Pesticides widely used in agriculture, such as paraquat (PQ) and diquat (DQ), are designed to increase yields; at the same time, it also causes environmental pollution and food toxicity due to the presence of pesticide residue, which seriously threatens the ecosystem and human health [1]. Thus, the identification and quantification of pesticide residues are essential to control environmental pollution and ensure public safety [2]. In recent years, instrumental methods for detecting pesticide residues are generally based on chromatographic and spectral methods [3], such as gas chromatography or high-performance liquid chromatography coupled with mass spectroscopy [4], fluorescence [5], surface-enhanced Raman scattering [6], and potentiometric [7]. These methods could achieve sensitive and specific recognition, but they generally involve tedious sample preparation, skillful operators, and expensive and sophisticated instruments, which is not convenient for in-field detection. Hence, it is necessary to develop a simple, reliable, and fast method for pesticide detection.

In an attempt to accomplish the goal mentioned above, the functionalized nanodevices and nanomaterials are highly desirable [8]. As one of the most widely used nanodevices, quartz nanopipettes have been utilized as a novel detection platform for various detection applications, owing to the advantage that it can be cheaply and reproducibly fabricated from quartz capillaries with a resolution of tens of nanometers. Compared to the usual capillary electrophoresis method [9], the nanopipette provides a more sensitive platform owing to its conical structure. However, to achieve

✉ Tao Ma
taoma01@wust.edu.cn

✉ Feng Liang
feng_liang@whu.edu.cn

1 The State Key Laboratory of Refractories and Metallurgy, School of Chemistry and Chemical Engineering, Wuhan University of Science and Technology, Wuhan 430081, People's Republic of China

2 Improve-WUST Joint Laboratory of Advanced Technology for Point-of-Care Testing and Precision Medicine, Wuhan University of Science and Technology, Wuhan 430081, People's Republic of China

3 College of Chemistry, Jilin University, Changchun 130012, People's Republic of China

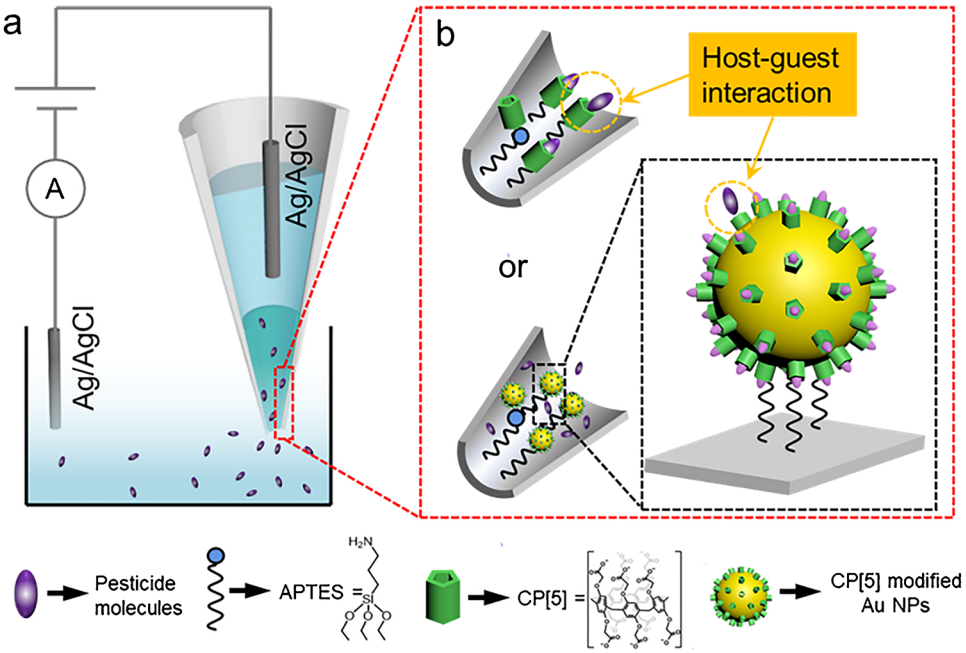

Scheme 1 Schematic illustration of silica nanopipette sensor based on host–guest interaction (not to scale). The schematic representation of **a** the measurement setup and **b** the recognition of pesticides based on host–guest interaction on the different functionalized inner surface of the nanopipette

satisfactory results with a higher ionic current response and lower limit of detection (LOD), most nanopipette-based devices need complex sample pretreatment and precise equipment such as patch-clamp amplifiers. Thus, a novel, portable nanopipette sensor capable of real-time, fast detection of target molecules is extremely desired for sensing applications.

Generally, the rational design of functionalized nanopipette determines the ceiling in sensitivity and selectivity of the sensor. Among the various constructing strategies of the functionalized nanopore, host–guest chemistry attracts tremendous attention for its recognition and analysis abilities due to its reversibility and selectivity for the specific substrate [10]. Several macrocyclic hosts with a hydrophobic cavity, such as cyclodextrin, cucurbituril, and pillararenes, have been used as functional molecules to improve the performance of nanopore-based sensors [11–14]. Caboxylatopillar[n]arenes (CP[n]) and their derivatives such as caboxylatopillar[5]arenes (CP[5]) [15] and carboxylated leaning pillar[6]arene (CLP[6]) [16], as the newest host molecules, process easy modification, and high tenability, and as such, are an ideal platform to design receptors. However, most of the reported research about nanopores based on host–guest interaction focused on the construction of functional gated switches rather than the potential of constructing high-performance sensors, due to the poor conductivity of macrocyclic molecules.

The long goal of our research group is to develop macrocyclic host-based metallic nanoparticles which could be used in catalysis, detection, and separation [17–22]. In this project, we demonstrated an Au NP-enhanced nanopipette sensor based on host–guest interaction for the sensitive and selective recognition of pesticide residuals (Scheme 1). The detection system was constructed by the condensation of an amino group of 3-aminopropyltriethoxysilane (APTES) immobilized on the nanopipette inner surface and the carboxyl group of CP[5] (or CLP[6]) adsorbed on Au NPs. When the pesticide molecules enter into the nanopipette, the macrocycles would recognize the guests [23], resulting in a significant variation of surface electronegativity, which could be determined by the ion current [24]. Based on the application of host–guest recognition and the gold nanoparticle enhance effects, this sensor platform not only demonstrated the specific recognition for PQ and DQ but also explore the size effects of gold nanoparticles and nanopores for the PQ detection sensitivity. The results revealed that the smaller CP[5]-Au NPs, the more sensitive; however, the size of the nanopore makes no difference for detection. The nanopipette sensor improved the detection limit to 3.4×10^{-11} mol/L and displayed a remarkable specificity toward PQ. This work paves the way to further develop diverse nanopipette host–guest recognition-based molecular sensors for the detection of small pesticides molecular in the fields of environment and food safety. Meanwhile, it also indicated a new strategy for detecting bioactive compounds in the field of chemistry and biology.

Experimental

Fabrication and functionalization of the nanopipette sensors

Nanopipettes were fabricated through a laser pipette puller according to previous reports [25], and the CP[5], CP[5]-modified Au NPs (CP[5]-Au NPs), CLP[6] and CLP[6]-modified Au NPs (CLP[6]-Au NPs) were prepared according to our reported procedures [15, 16, 23].

And, all of the materials and instruments involved in this work were shown in Section 1 of supplementary information (SI). The functionalized nanopipettes were modified in 2 steps: (1) the nanopipettes were backfilled with 20% (v/v) APTES ethanol solution, followed by incubation in a partially sealed beaker placed in a vacuum desiccator for 6 h at room temperature. Then, APTES-modified nanopipettes (APTES-nanopipette) were obtained after thoroughly washing with ethanol and drying in a vacuum desiccator at room temperature for 2 h. The amino (-NH_2) groups of APTES-modified nanopipette inner surface were used as an anchor to further functionalization. (2) Five milliliters of CP[5] (CLP[6], CP[5]-Au NPs, or CLP[6]-Au NPs respectively solution (0.25 mM) containing 23 mg of EDC-HCl and 14 mg of NHS was added into the APTES-nanopipette. After that, the modified nanopipette sensors were constructed by a classical EDC/NHS cross-linking reaction [14] between -NH_2 and carboxyl (-COOH) groups of CP[5] (or CLP[6]) for 24 h. Finally, the as-prepared nanopipette sensors were obtained after washing and vacuum desiccation at room temperature for 2 h.

Electrochemical characterization

The electrochemical experiments were carried out using the classical two-electrode system [26] with an electrochemical workstation (CHI 660E). In detail, current–voltage (*I-V*) measurements were performed for characterization and detection processes by sweeping the voltage from − 1 to + 1 V at a scan rate of 50 mV/s. KCl aqueous solution (10 mM) was served as the electrolyte inside and outside of nanopipette sensors. Two Ag/AgCl wires were placed in the nanopipettes and the electrolyte as working and counter/reference electrodes, respectively. The infilled supporting solution of the nanopipettes and the electrolyte in the electrolytic cell were kept the same throughout the experiments. Each test was repeated 6 times to obtain the average current value at different voltages. The rectification ratio r ($r = |I_-/I_+|$, where I_+ and I_- refer to the ionic current at the bias voltage of + 1 V and − 1 V, respectively) was used to represent the rectification status of the nanopipettes [26]. To avoid current differences between different nanopipettes, a normalized current change ($\Delta I/I_0$, where $\Delta I = I - I_0$, I and I_0 represent the ionic current after and before the incubation at the bias voltage of − 1 V, respectively) was employed to translate the ionic current response to detection capability of different functionalized systems.

Detection of paraquat in real sample

To evaluate the feasibility of CP[5]-Au NP-modified nanopipette sensor for detection of PQ, for the real water samples, tap water from the lab in Wuhan University of Science and technology, river water from the Yangtze River (Wuhan), and lake water from East Lake (Wuhan) were selected and then filtered with 0.22-μm microfiltration membranes before the sensing detection. The fruit and tea samples obtained from Zhongbai supermarket in Wuhan were processed by standard extraction methods before analysis [27, 28]. The performance of 3 nm CP[5]-Au NP-modified nanopipette for PQ detection in real samples was confirmed by a spiking experiment. The detail of real sample detection is shown in Section 7 of supplementary information.

Results and discussion

Fabrication of host–guest based nanopipette sensors

The quartz nanopipette was fabricated by a laser puller instrument with a tip diameter of 72 nm (Fig. S1). To achieve the sensitive detection of pesticides, CP[5] which can recognize positively charged molecules was introduced into the nanopipette. As shown in Fig. 1a, firstly, the sensor was constructed by covalently immobilizing the APTES on the inner wall of the nanopipette. Then, the APTES acts as a linker to bond with the CP[5] through condensation of the amino and carboxyl groups. Thus, the pesticide molecules could be recognized by CP[5]-functionalized nanopipette via host–guest interaction, resulting in a significant variation of charge on the surface, which could be measured by the ratio of ionic current change. Therefore, a functional nanopipette sensor based on host–guest recognition was constructed for pesticide molecule detection.

It is well known that the charge on the inner surface of the nanopipette could strongly affect the ion current rectification (ICR) ratio r when the polarity is reversed [29, 30]. That is, when $r < 1$, the nanopipette is anion-selective and the inner surface charge is positive. When $r > 1$, the nanopipette is cation-selective and the inner surface charge is negative [31]. To monitor the modification process of the nanopipette, the change of r was measured in KCl solution (10 mM). As shown in Fig. 1b, the original nanopipette showed a nonlinear *I–V* curve (black plots) with an r of 2.83. Because of the conical shape and presence of inherent anionic hydroxyl groups, nanopipettes can preferentially transport cations (K^+) from the entrance to the inside when the potential was applied. After modification with APTES, there was an obvious inversion of the rectifying characteristics ($r = 0.30$), indicating the successful modification by APTES resulted in a change in the

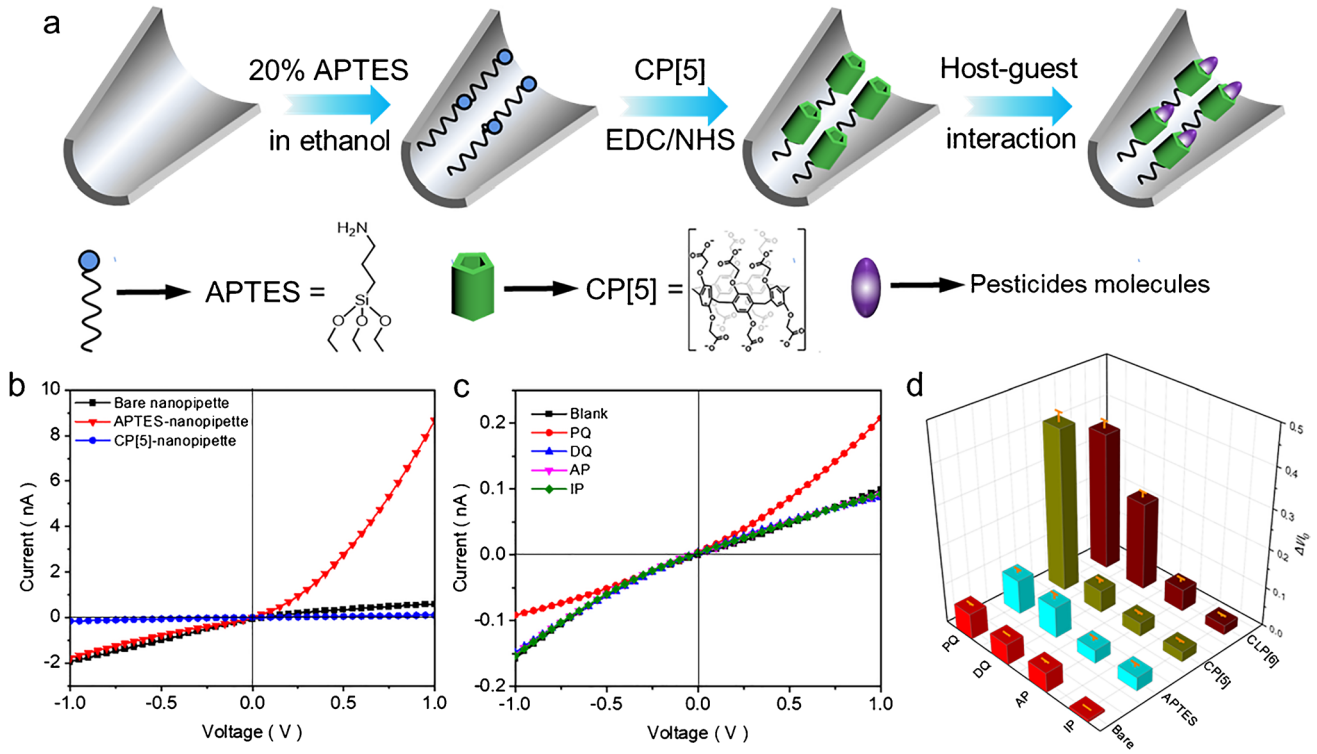

Fig. 1 **a** Schematic of fabrication of CP[5]-modified nanopipette sensor based on the host–guest interaction for pesticide molecules detection; **b** *I–V* curves of the glass nanopipette (in 10 mM KCl with a scan rate of 50 mV/s and range of − 1 and + 1 V) at various stages of functionalization process: Bare (black plots), modified with APTES (red plots), and modified with CP[5] (blue plots); **c** *I–V* curves of the CP[5]-nanopipette in the presence of 400 nM PQ, DQ, AP, and IP in 10 mM KCl electrolyte; **d** histogram of ionic current change ratios ($\Delta I/I_0$) of bare, APTES, CP[5], and CLP[6]-modified nanopipettes at − 1 V in 10 mM KCl electrolyte containing 400 nM different pesticide molecules. The number of experiments is six ($n = 6$)

polarity of the inner surface of the nanopipette from negative to positive (red plots in Fig. 1b). Subsequently, CP[5]-modified nanopipette (CP[5]-nanopipette) was prepared by connecting carboxylates of CP[5] and amino groups of APTES modified on nanopipette through amide bonds. The rectifying characteristic returned to the initial state of cation (K^+) selectivity ($r = 1.12$) due to the negative charges coming from the carboxyl groups of CP[5]. Furthermore, the ionic current of CP[5]-nanopipette decreased dramatically at − 1 V compared with that of bare nanopipette, which was owing to successful modification of CP[5] resulting in decreased negative charge and enhanced hydrophobicity on nanopipette inner surface [32]. Due to the difficulty of measuring a quartz nanopipette directly, the characterization of the functionalized inner surface was approximated by measuring the contact angles (CA) of quartz sheets using the same modified procedure (shown in Fig. S2).

To evaluate the feasibility of nanopipette sensors for pesticide detection, paraquat (PQ), diquat (DQ), acetamiprid (AP), and imidacloprid (IP) were added to the electrolyte, respectively. As a control, the *I–V* curves of bare nanopipette and APTES-nanopipette exposed to KCl electrolytes containing 400 nM PQ, DQ, AP, and IP respectively were obtained in Fig. S3a and b. The similar *I–V* curves in each result suggested that both nanopipettes have no responsibility for added molecules. While Fig. 1c showed the selectivity of the CP[5]-nanopipettes for PQ. The *I–V* curve with an *r* of 0.43 in the presence of PQ evidently differs from that of others (the *r* is 1.59, 1.68, 1.65, and 1.64 for blank, and in the presence of DQ, AP, and IP respectively). In addition, at − 1 V, the ion current decreases in the presence of PQ, whereas it is kept at a constant in the presence of other pesticide molecules. The above results strongly illustrated that the positively charged PQ molecules were captured by CP[5] through host–guest recognition [15] when it crossed the nanopore and resulting in a positively charged inner surface. Meanwhile, the CP[5]-nanopipette showed no response for DQ, AP, and IP molecules owing to the CP[5]'s small size, which makes it difficult to distinguish larger molecules, even though some are positively charged (shown in Fig. S4). Therefore, the CP[5]-functionalized nanopipette sensor exhibits a high-selectivity response for PQ.

To gain more about nanopipette sensors based on host–guest interactions, CLP[6] was also introduced into nanopipette (CLP[6]-nanopipette) as a host to detect pesticide molecules due to its larger cavity size and more sensitive

for recognition [16]. Fig. S5a depicts the *I–V* curves of bare nanopipettes and APTES or CLP[6]-functionalized nanopipettes, revealing that CLP[6] was successfully modified on the inner surface of nanopipettes. The presence of PQ and DQ resulted in an obvious decrease in the ion flux across the CLP[6]-nanopipette, whereas the current is nearly constant in the presence of other molecules. This can be ascribed to the CLP[6] having a stronger affinity for PQ and DQ than other tested molecules [16]. Thus, other pesticide molecules cannot change the inner surface properties of the nanopipette. The current change ratio ($\Delta I/I_0$) at − 1 V was determined to quantify the changes when the ions across different functionalized nanopipettes are in the presence of pesticide molecules. In comparison to the current ratios obtained from the bare nanopipette and APTES-nanopipette (Fig. 1d), CP[5]-nanopipette acted as a good selectivity binding site for PQ, while the CLP[6]-nanopipette demonstrated reasonable recognition for both PQ and DQ due to specific macrocycle recognition [23]. Overall, these results strengthened the idea that both CP[5]-nanopipette and CLP[6]-nanopipette have a great potential for pesticide detection.

The enhanced sensitivity of host–guest–based nanopipette sensors by gold nanoparticles

Supramolecular recognition of CP[5] and CLP[6] for pesticide molecules is a feasible approach in electrochemical sensors, but the low electrical conductivity limits their sensitivity [32]. As shown in Fig. 1b, after modification of CP[5], the current at − 1 V drastically decreased to − 0.16 nA, which is not favorable in achieving the higher-sensitive detection. Thus, the CP[5]-modified gold nanoparticles (CP[5]-Au NPs) were employed to enhance the sensitivity of nanopipette sensors (shown in Fig. 2a), due to the signal magnification effects of Au NPs in sensing [33]. According to our previous works [15], CP[5]-Au NPs were generated by reducing the $HAuCl_4$ with $NaBH_4$ in the presence of CP[5], which had a high dispersibility (Fig. S6a) and small size with narrow size distributions of 11 ± 1.5 nm (Fig. S6b). Furthermore, the HRTEM image (inset in Fig. S6a) indicates that CP[5]-Au NPs had well-defined crystalline with interplanar *d* spacings of 2.36 and 2.05 Å, corresponding to the (111) and (200) planes of face-centered cubic Au [15].

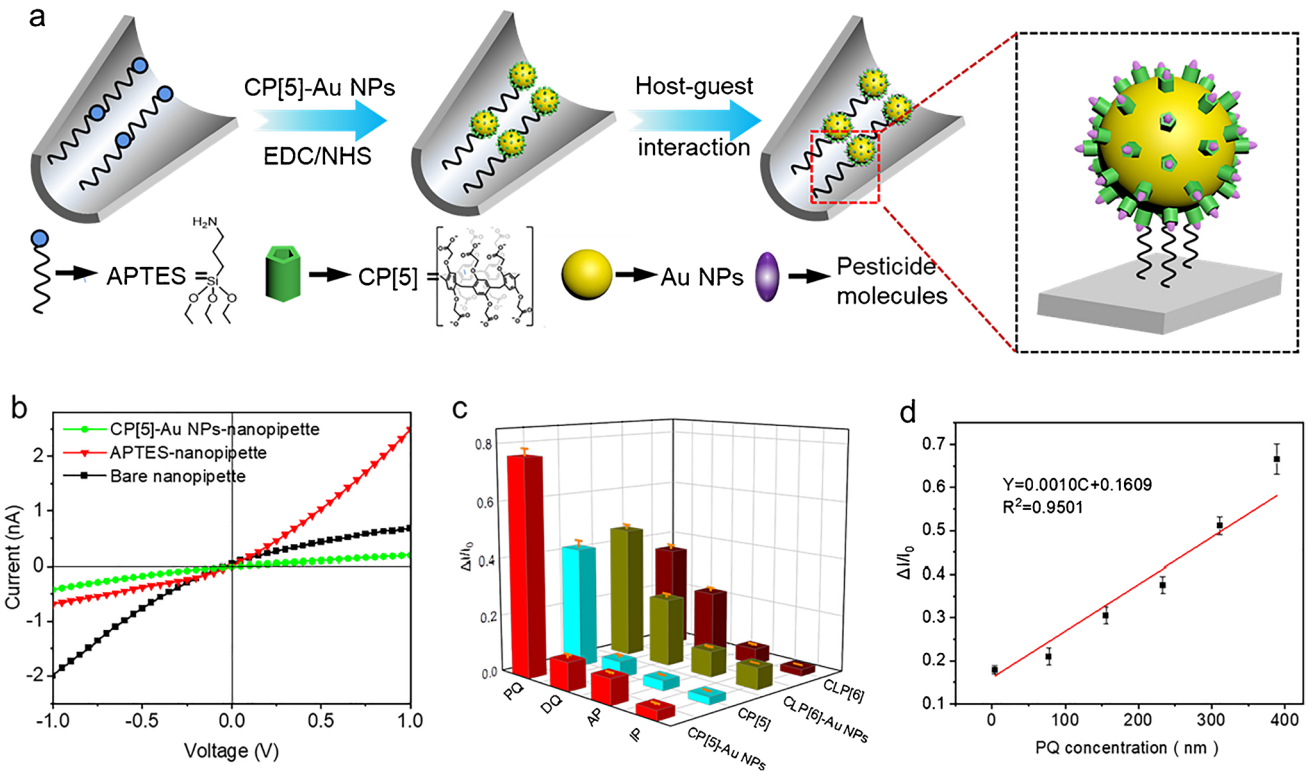

Fig. 2 **a** Schematic of the fabrication of CP[5]-Au NP-modified nanopipette sensor based on the host–guest interaction for the pesticide molecules detection. **b** *I–V* curves of bare nanopipette (black plots), APTES-modified nanopipette (red plots), and CP[5]-Au NPs modified nanopipette (green plots), using 10 mM KCl as electrolyte. **c** Histogram of ionic current change ratios ($\Delta I/I_0$) of CP[5], CP[5]-Au NPs, CLP[6], and CLP[6]-Au NP-modified nanopipettes at − 1 V in 10 mM KCl electrolyte containing 400 nM different pesticide molecules. **d** The relationship between the ionic current change at − 1 V and the PQ concentration (detected by CP[5]-Au NPs-nanopipette). ($n = 6$, for **c** and **d**)

Similar to the CP[5]-nanopipette, CP[5]-Au NP-modified nanopipette (CP[5]-Au NPs-nanopipette) was also constructed by amide bonds. The decreased CAs following CP[5]/CLP[6]-Au NPs modification compared to previous data, as shown in Fig S7, confirmed the method's viability. Furthermore, the SEM images of the nanopipette tip before (Fig. S8a) and after (Fig. S8b) cutting off indicated the successful modification. Fourier transform IR spectroscopy (FTIR) of different functionalized nanopipettes and corresponding molecules were shown in Fig. S9 to confirm that CP[5]-Au NPs were indeed modified on the nanopipette. The presence of typical Si–O-Si stretching mode at 1150 cm^{-1} [34] as well as the C = O bond of carboxyl groups at 1800 cm^{-1} [35], and the absence of the -NH_2 mode at 1620 cm^{-1} [36] demonstrated the successful functionalization of CP[5]-Au NPs on APTES-modified nanopipette. XPS spectrum of Au 4f and N 1 s (Fig. S10) further confirmed the presence of CP[5]-Au NPs on the nanopipette inner surface.

As shown in Fig. 2c, compared with the *r* of APTES-nanopipette (0.27), the CP[5]-Au NPs-nanopipette had an *r* of 2.16, which suggests that the inner nanopipette surface was negative. Meanwhile, the ICR direction was also reversed due to the successful incorporation of the negatively charged carboxyl group from CP[5]-Au NPs. It should be noted that the rectification properties of CP[5]-Au NPs-nanopipette was stronger than that of CP[5]-nanopipette ($r = 1.59$, shown in Fig. 1c.), owing to the asymmetric structure of the inner surface of the nanopipette after the induction of Au NPs [37]. Additionally, in contrast to the weak onset current of CP[5]-nanopipette (− 0.16 nA at − 0.1 V shown in Fig. 1c), CP[5]-Au NPs-nanopipette could achieve − 0.42 nA, as a consequence of superior conductivity of Au NPs. Taken together, these results indicate that the introduction of Au NPs indeed enhances the rectification properties and sensitivity of functionalized nanopipette, which can contribute to the higher selectivity and lower detection limits for pesticide molecules.

The normalized current changes ($\Delta I/I_0$) were obtained to interpret the ionic current response to pesticide molecules while using different nanopipette sensors. As shown in Fig. 2c, the CP[5]-Au NPs-nanopipette showed the highest selectivity to PQ ($\Delta I/I_0 = 0.76$) and a very low response to DQ ($\Delta I/I_0 = 0.1$), AP($\Delta I/I_0 = 0.09$), and IP($\Delta I/I_0 = 0.03$). Remarkably, the response of CP[5]-Au NPs-nanopipette to PQ is 81% higher than that of CP[5]-nanopipette. This suggested that the introduction of Au NPs indeed enhances the selectivity and sensitivity of CP[5]-functionalized nanopipette for PQ detection. Modification of CP[5]-Au NPs on nanopipette not only improved the conductivity of nanopipette but also enlarged the area of the inner surface that can provide more CP[5] sites to capture guest molecules. To illustrate the Au NPs enhancement effect, the CLP[6]-Au NP-modified nanopipette (CLP[6]-Au NPs-nanopipette) was also prepared (Fig. S11). In comparison with CLP[6]-nanopipette, the current response of nanopipette integrated CLP[6]-Au NPs resulted in a 29% improvement for PQ, but a negligible influence for DQ (Fig. 2c). Thus, the introduction of Au NPs into CLP[6]-nanopipette also plays a role in improving sensitivity for PQ. Although CLP[6]-Au NPs-nanopipette has an obvious response for both PQ and DQ, the current change ratio for PQ is around two times higher than that for DQ, which can be used to distinguish them. Nonetheless, the CP[5]-Au NPs-nanopipette exhibited a more outstanding Au NPs enhancement effect and higher selectivity for PQ than that of CLP[6]-Au NPs-nanopipette. Therefore, the further investigation of CP[5]-Au NPs-nanopipette for PQ detection was deeply explored in a later discussion.

Water-soluble CP[5] is an organic anion due to the deprotonation of the carboxyl group and exhibited a high association constant for PQ ($K = (8.2 \pm 1.7) \times 10^4$ M), which is 70 times higher than that of a complex formed between paraquat and perhydroxylated pillar[5]arene. When paraquats are across the rim of the nanopipette, they were captured by CP[5] through host–guest interaction with high binding affinity, and the negatively charged inner surface becomes positive. Hence, according to the different charge density of the inner wall depending on the quantity of paraquat captured by CP[5], the different current change ratios were obtained to represent different paraquat concentrations. Figure 2d showed the relationship between $\Delta I/I_0$ detected by CP[5]-Au NPs-nanopipette and the series concentration of PQ. The $\Delta I/I_0$ monotonously increased with PQ concentration from 0 to 400 nM, with unsaturation and a limit of quantitation (LOQ) of 4 nM, which also can be seen in *I–V* curves (Fig. S7). The linear regression equation was $\Delta I/I_0 = 0.0010c + 0.1609$ with a regression correlation coefficient of 0.9501. Then, the limit of detection (LOD) of CP[5]-Au NPs-nanopipette sensor for PQ was calculated to 0.73 nM, based on the formula (LOD = 3σ/slope), where σ is the standard deviation of blank solution and with a value of 0.000245 in this experiment [32, 38]. The LOD of CLP[6]-Au NPs-nanopipette for PQ and DQ were also respectively obtained with values of 1.7 and 4.5 nM according to the linear regression equation simulated from Fig. S13. It is worth mentioning that the LOD of CP[5]-Au NPs-nanopipette for PQ is much lower than that of other reported methods (Table S2). It would be expected that the increased sensitivity benefited from the high susceptibility of Au NPs supported macrocyclic molecules toward the guest molecules.

Optimization and anti-interference of CP[5]-Au NPs-nanopipette sensor for PQ

Although the CP[5]-Au NPs-nanopipette sensor exhibited an excellent LOD for PQ, there is still much room for

improvement. The size and functional molecules loading rate of the nanopipette has a critical role in detection [33]. Thus, the size effects of nanopipette and CP[5]-Au NPs were further discussed. Because the low LOQ of CP[5]-Au NPs-nanopipette with a value of 4 nM has been achieved, a higher LOQ standard of 0.04 nM was artificially set to make a preliminary judgment on whether or not the optimization was achieved.

Firstly, the size effect of the nanopipette was investigated. As shown in Fig. S14, a series of quartz nanopipettes with different sizes were produced by setting the corresponding parameters on a laser puller instrument (Table S1). Interestingly, the current at − 1 V decreased as decreased nanopipette tip diameters because the smaller nanopore induces the larger resistance [39]. Therefore, the larger nanopipette may have a higher sensitivity for ion current. However, as shown in Fig. S14g, h, and i, although they were good for the detection of PQ with a higher concentration (400 nM), all of three CP[5]-Au NPs-nanopipettes were not effective for the detection of PQ with low concentration (0.04 nM). Hence, the results of this experiment illustrated that the LOQ appeared to be barely affected by the size of the nanopipette. In addition, the ionic current change ratios ($\Delta I/I_0$) of 70-nm nanopipettes are the highest in presence of 400 nM PQ (see in Fig S15) and suggest the best response for PQ detection in four nanopipettes, Thus, 70-nm nanopipette was chosen for later exploration.

To gain the insights into size effects of CP[5]-Au NPs on the detection sensitivity of the nanopipette (70 nm used here) sensor for PQ, the CP[5]-Au NPs with other three different sizes were prepared by simply varying the precursor solution concentration. Figure 3a displayed a series of TEM images of CP[5]-Au NPs with different diameters. From the size distribution shown in Fig. S16, the size of CP[5]-Au NPs were 3.0 ± 0.7 nm, 7.1 ± 0.9 nm, 11.0 ± 1.5 nm (used in The enhanced sensitivity of host–guest-based nanopipette sensors by gold nanoparticles), and 19.0 ± 1.6 nm, which corresponding to the nanoparticles in Fig. 3a (i), (ii), (iii), and (iv). Correspondingly, the UV–vis absorption peak increased gradually from 505 to 511, 519, and 528 nm with the growing CP[5]-Au NPs size. The *I–V* curves of bare, APTES modified, or CP[5]-Au NPs of various size-modified nanopipettes were also analyzed in Fig. S17. The rectifying ratio of the nanopipette was larger than 1 after 3 nm or 7 nm CP[5]-Au NP modification compared with that of the APTES-nanopipette ($r < 1$). Nevertheless, the r of 19 nm CP[5]-Au NPs-nanopipette was barely distinguished from that of APTES-nanopipettes. The results above indicate that only the smaller size CP[5]-Au NPs could be modified on the inner surface of the nanopipette, and the 19-nm CP[5]-Au NPs were too large to be modified on. Hence, the CP[5]-Au NPs with smaller sizes may make difference in boosting the sensitivity of nanopipette sensors.

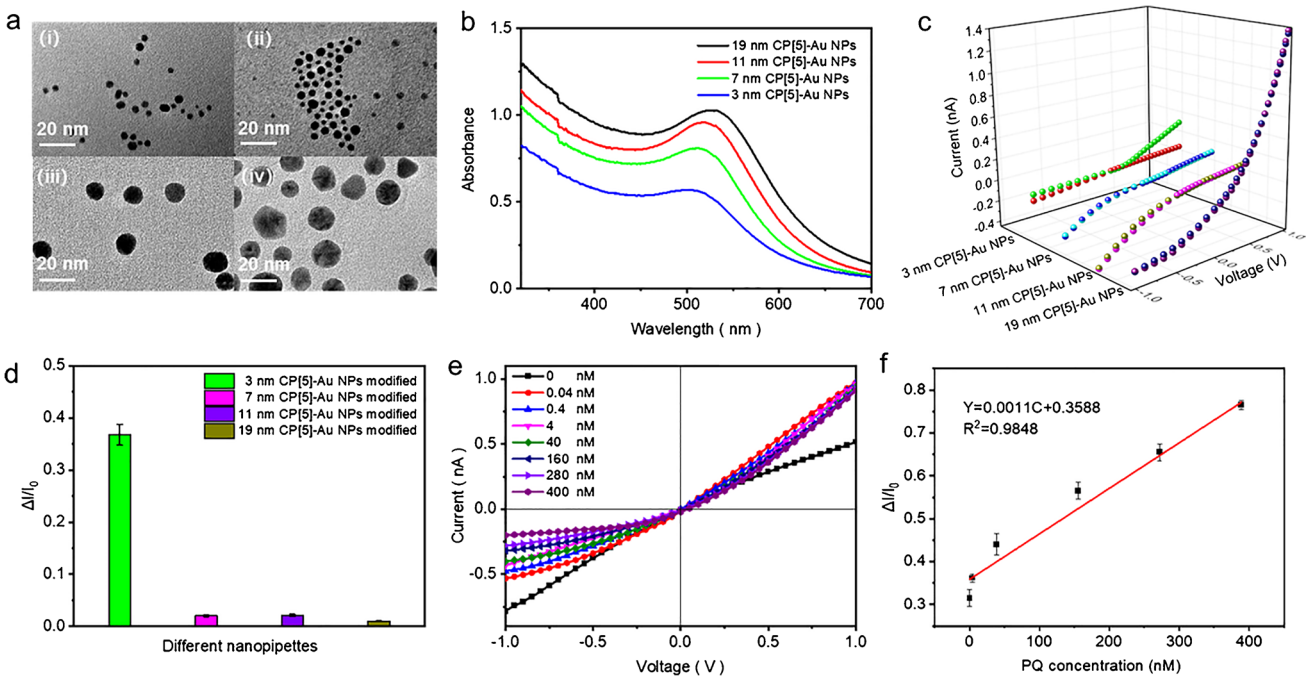

Fig. 3 **a** TEM images of CP[5]-Au NPs with different sizes: (i) 3.0 nm, (ii) 7.1 nm (iii), 11.0 nm, (iv) 19.0 nm. **b** UV–vis spectrum of different CP[5]-Au NPs. **c** $I-V$ curve of the different CP[5]-Au NP-modified nanopipettes before and after the addition of 0.04 nM PQ. **d** Histogram of ionic current change ratios ($\Delta I/I_0$) of different CP[5]Au NP-modified nanopipettes at − 1 V in the presence of 0.04 nM PQ. **e** *I–V* curves of the 3-nm CP[5]-Au NP-modified nanopipette under the addition of various PQ concentrations. **f** The relationship between $\Delta I/I_0$ and PQ concentration. All the electrochemical tests were in 10 mM KCl electrolyte. $n = 6$ for **d**, **e**, and **f**

I–V curve changes (Fig. 3c) and corresponding $\Delta I/I_0$ (Fig. 3d) of nanopipette sensors modified with CP[5]-Au NPs of different sizes were obtained before and after the addition of 0.04 nM PQ. What stands out is that only modified with 3 nm CP[5]-Au NPs, the nanopipette exhibited an obvious response for PQ (green plots). And, the $\Delta I/I_0$ of 3-nm CP[5]-Au NPs-nanopipette was achieved at 0.37 (Fig. 3d). The observed outstanding performance of 3-nm CP[5]-Au NP-modified nanopipette could be attributed to the highly abundant CP[5] sites that benefit to recognize the PQ even at extremely low concentrations. Typically, the smaller size of nanoparticles subjects them to a higher loading rate of macrocyclic hosts and less steric hindrance on the surface modification [40]. In this case, the CP[5]-Au NPs with smaller sizes are easier to be modified on the nanopipette inner surface and allow for more binding sites of macrocyclic hosts on the same surface area. The as-prepared 3-nm CP[5]-Au NPs-nanopipettes were then used for PQ sensing with different PQ concentrations (from 0 to 400 nM, shown in Fig. 3e). With the growth of PQ concentration, the $\Delta I/I_0$ increased gradually and displayed a good linear relationship to PQ concentration with a fitted equation of $\Delta I/I_0 = 0.0011c + 0.3588$. The LOD of 3-nm CP[5]-Au NPs-nanopipette sensor for PQ was also calculated to be 0.034 nM, which is more than one order of magnitude higher than that of 11 nm CP[5]-Au NPs-nanopipette. Therefore, the goal of optimizing the CP[5]-Au NP-modified nanopipette sensor mentioned at beginning of this section could be achieved by decreasing the size of CP[5]-Au NPs. Compared with other methods (as shown in Table S2), 3-nm CP[5]-Au NPs-nanopipette exhibited the best LOD and a wider dynamic linear range for PQ detection.

As shown in Fig. S18, either without or with PQ in the electrolyte, all the curves at scan rates of 10, 30, 50, 70, and 90 mV/s displayed a high degree of overlap, suggesting the scan rate scarcely affected the experimental result. Usually, the moderate scan rate of 50 mV/s is used [14, 41]. The influence of solution pH on the detection was investigated by deionized (DI) water-KOH/HCl solution ranging from 3 to 11. In absence of PQ, the ion current at − 1 V decreased with increasing acidity (Fig. S19a), owing to the protonation of the carboxylic group on CP[5]. In particular, the deflection of *r* at acid environment compared with that at KCl solution (pH = 7) further confirms the positively charged inner surface of the nanopipette. Fig. S19b to f shows the results of PQ detection at a different pH. Remarkably, nanopipette makes no response for PQ added at pH = 3 or 5 (Fig. S16b, c), whereas, with a strong signal at pH = 7, 9, and 11 (Fig. S19d, e, and f), because of the presence of more protonated carboxyl at an acid solution, and more deprotonated carboxyl (which could enhance the capture capacity for positively charged) in alkaline solution. In addition, the initial current at − 1 V, either in the absence (corresponding to I_0) or presence (corresponding to *I*) of PQ, decreased with the increasing pH when pH ≥ 7. The influence of I_0 is caused by negatively charged density inner surface of nanopipette, while that of *I* results from enhanced recognition of more deprotonated carboxyl group on CP[5]. Although both reasons originated from pH, the former is more dramatically affected by pH variations; thus, $\Delta I/I_0$ also decreased with increasing pH. Therefore, pH = 7 (KCl solution without buffer) was chosen in the following measurements.

The anti-interference of 3-nm CP[5]-Au NPs-nanopipette was investigated by changing the scan rate and adjusting interfering substance including metal ions and other pesticides. Fig. S20 shows *I–V* curves of 3-nm CP[5]-Au NPs-nanopipette exposed to electrolytes containing 400 nM carbaryl, metamitron, isocarbophos, and atrazine (Fig. S20a) or 50 nM Ni^{2+}, Zn^{2+}, Ca^{2+}, and Cu^{2+} (Fig. S20b). The presence of PQ resulted in a drastic decrease in the ion flux across the nanopipette, whereas the current is nearly constant in presence of the other tested pesticides and ions. This can be ascribed to the CP[5] of nanopipette having a stronger affinity for PQ and an outstanding anti-interfering for metal ions and other pesticides.

Detection of paraquat in real sample

In this part, to assess the viability of the tested system for the detection of PQ in the real world, real sample analyses were processed using 3-nm CP[5]-Au NPs-nanopipette. Spiking was carried out at the beginning of the whole analytical process. And, the PQ standard (no more than 10 μg/L (about 40 nM)) of drinking water from the World Health Organization (WHO) was used as a reference [42]. Firstly, the tap water and natural water collected from the Yangtze River (Wuhan, China) and the East Lake (Wuhan, China) were detected with the 3-nm CP[5]-Au NPs-nanopipette sensor, respectively. Upon adding selected water samples, the sensing system did not produce an obvious reversal signal of rectification (black lines in Fig. S21) comparing DI water adding (black line in Fig. 3e), which suggests the PQ level in the obtained samples is lower than the detection limit of the sensor due to the diluted effect involved in the ecosystem. To further validate the feasibility of the sensor, the spike-and-recovery experiments using tap, river, and lake water as an example of real samples were performed, and the results were summarized in Table S4. Despite the concentration of PQ in collected water is much lower (0.2 nM) than that from WHO (about 40 nM), the obvious response for PQ can still be consistently identified by this sensor. Additionally, the recoveries for PQ were in the range of 92.0–106% with the relative standard deviations less than 7.4%. These results indicated the proposed method was reliable and practical for the detection of PQ in real environmental water samples.

The PQ detection of apple and tea sample was also explored. The apple and tea were purchased from a local supermarket (Wuhan, China). The matrix effects of the apple and tea samples are always complicated. In order to obtain the accurate content of PQ in the real sample, the method of extraction-dryness-redissolution (see detail in Section 7 of SI) [27, 28] was employed to obtain the original liquid for later experiment, including the blank sample without PQ and experimental sample with PQ added (about 400 nM and 4000 nM in apple and tea original liquid, respectively). Firstly, *I–V* curves maintained constant when a different volume of the blank sample of apple and tea samples added to the electrolyte (Fig. S22) suggested that the PQ concentration in apple and tea is too low to be detected. Hence, the spike-and-recovery experiments using blank samples were also employed here. As shown in Fig. S23, linear relationship between $\Delta I/I_0$ and PQ concentration of $\Delta I/I_0 = 0.0015c + 0.2955$ for apple detection, and $\Delta I/I_0 = 0.0008c + 0.2771$ for tea detection were obtained with high-correlation coefficient, when the sensor exposed in electrolyte with different PQ concentrations. A series of volume of experimental samples of apple and tea were added to 5 mL electrolyte to detect the PQ concentration (Fig. S24). Recovery results accordingly relationship above were summarized in Table S5. The measured recoveries were around 90% ($n = 6$) with the RSD less than 5.0%, which suggests the sensor is accurate and reliable and can be used for quantification of PQ in the practical sample. Lastly, HPLC was used as a reference to determine accurately the concentration of PQ present in real samples (see Section 7.3 in SI), because HPLC is considered to be reliable and highly accurate. As shown in Fig S25 and Table S6, the PQ in the real sample without spiking were not detected by neither nanopipette sensor nor HPLC, while the recovery and RSD of tea and apple samples with spiking obtained from nanopipette sensor and HPLC were similar, which confirmed the accuracy of our nanopipette sensor is sufficient.

Conclusions

A functionalized nanopipette sensor for extremely sensitive and selective PQ detection was developed by employing CP[5] to capture free PQ via host–guest interaction and Au NPs to improve sensing performance. The nanopipette sensor demonstrated a low detection limit, a broad detection range, and a high selectivity for PQ over other interfering substances. When compared to previously described techniques, this strategy for PQ detection is highly sensitive, simple to use, and quite efficient. Furthermore, the feasibility of the proposed 3-nm CP[5]-Au NPs-nanopipette has been proven by the determination of paraquat in real environmental water samples with satisfactory results. Hence, the gold nanoparticles enhanced nanopipette sensors based on host–guest interaction appear to hold great practical potential for the detection of small molecules in the field of food safety and medicine.

Supplementary Information The online version contains supplementary material available at https://doi.org/10.1007/s00604-022-05348-9.

Funding This work was supported in part by grants from the National Natural Science Foundation of China (21871108), the Program for Innovative Teams of Outstanding Young and Middle-Aged Researchers in the Higher Education Institutions of Hubei Province (T201702). The authors also thank Shiyanjia Lab (www.shiyanjia.com) for the support of the XPS test.

Declarations

Conflict of interest The authors declare no competing interests.

References

1. Seiber JN, Kleinschmidt LA (2011) Contributions of pesticide residue chemistry to improving food and environmental safety: past and present accomplishments and future challenges. J Agric Food Chem 59:7536–7543
2. Zhang K, Li H, Wang W, Cao J, Gan N, Han H (2020) Application of multiplexed aptasensors in food contaminants detection. ACS Sens 5:3721–3738
3. Narenderan ST, Meyyanathan SN, Babu B (2020) Review of pesticide residue analysis in fruits and vegetables. Pre-treatment, extraction and detection techniques. Food Res Int 133:109141
4. Kuitio C, Klangprapan S, Chingkitti N, Boonthavivudhi S, Choowongkomon K (2021) Aptasensor for paraquat detection by gold nanoparticle colorimetric method. J Environ Sci Health B 56:370–377
5. Levine M (2021) Fluorescence-based sensing of pesticides using supramolecular chemistry. Front Chem 9:616815
6. Zhang D, Liang P, Yu Z et al (2020) Self-assembled "bridge" substance for organochlorine pesticides detection in solution based on surface enhanced Raman scattering. J Hazard Mater 382:121023
7. Arduini F, Cinti S, Scognamiglio V, Moscone D (2016) Nanomaterials in electrochemical biosensors for pesticide detection: advances and challenges in food analysis. Microchim Acta 183:2063–2083
8. Dergunov SA, Kim MD, Shmakov SN, Pinkhassik E (2019) Building functional nanodevices with vesicle-templated porous polymer nanocapsules. Acc Chem Res 52:189–198
9. Lanaro R, Costa JL, Fernandes LCR, Resende RR, Tavares MFM (2011) Detection of paraquat in oral fluid, plasma, and urine by capillary electrophoresis for diagnosis of acute poisoning. J Anal Toxicol 35:274–279
10. Meng FN, Yao X, Ying YL, Zhang J, Tian H, Long YT (2015) Single-molecule analysis of the self-assembly process facilitated by host-guest interactions. Chem Commun 51:1202–1205
11. Luo L, Nie G, Tian D, Deng H, Jiang L, Li H (2016) Dynamic self-assembly adhesion of a paraquat droplet on a pillar[5]arene surface. Angew Chem Int Ed 55:12713–12716
12. Ping G, Wang Y, Shen L et al (2017) Highly efficient complexation of sanguinarine alkaloid by carboxylatopillar[6]arene: pK_a shift, increased solubility and enhanced antibacterial activity. Chem Commun 53:7381–7384

13. Zhang G, Zhu X, Miao F, Tian D, Li H (2012) Design of switchable wettability sensor for paraquat based on clicking calix[4]arene. Org Biomol Chem 10:3185–3188
14. Zhang F, Ma J, Sun Y et al (2016) Fabrication of a mercaptoacetic acid pillar[5]arene assembled nanochannel: a biomimetic gate for mercury poisoning. Chem Sci 7:3227–3233
15. Li H, Chen DX, Sun YL et al (2013) Viologen-mediated assembly of and sensing with carboxylatopillar[5]arene-modified gold nanoparticles. J Am Chem Soc 135:1570–1576
16. Wang X, Wu JR, Liang F, Yang YW (2019) In situ gold nanoparticle synthesis mediated by a water-soluble leaning pillar[6]arene for self-assembly, detection, and catalysis. Org Lett 21:5215–5218
17. Chatterjee S, Lou X-Y, Liang F, Yang Y-W (2022) Surface-functionalized gold and silver nanoparticles for colorimetric and fluorescent sensing of metal ions and biomolecules. Coord Chem Rev 459:224461
18. Zhang M, Zhang H, Jin L et al (2022) Evidenced cucurbit[n]uril-based host-guest interactions using single-molecule force spectroscopy. Chem Commun 58:1736–1739
19. Wang R, Qian G, Guo J et al (2022) Nanocollision mediated electrochemical sensing of host-guest chemistry at a nanoelectrode surface. Faraday Discuss 233:222–231
20. Zhang H, Huang K-T, Ding L et al (2021) Electrochemical determination of paraquat using a glassy carbon electrode decorated with pillararene-coated nitrogen-doped carbon dots. Chin Chem Lett 33:1537–1540
21. Yang Q, Xu W, Cheng M et al (2022) Controlled release of drug molecules by pillararene-modified nanosystems. Chem Commun 58:3255–3269
22. Xu W, Cheng M, Zhang S et al (2021) Recent advances in chiral discrimination on host-guest functionalized interfaces. Chem Commun 57:7480–7492
23. Zhang H, Wang X, Huang KT, Liang F, Yang YW (2021) Green synthesis of leaning tower[6]arene-mediated gold nanoparticles for label-free detection. Org Lett 23:4677–4682
24. Cai SL, Cao SH, Zheng YB, Zhao S, Yang JL, Li YQ (2015) Surface charge modulated aptasensor in a single glass conical nanopore. Biosens Bioelectron 71:37–43
25. Wang Z, Liu Y, Yu L, Li Y, Qian G, Chang S (2019) Nanopipettes: a potential tool for DNA detection. Analyst 144:5037–5047
26. Liu G-C, Chen W, Gao M-J, Song L-B, Hu X-Y, Zhao Y-D (2018) Ion-current-rectification-based customizable pH response in glass nanopipettes via silanization. Electrochem Commun 93:95–99
27. Hou R-Y, Zhu X-J, Zhang Z-Z, Cai H-M, Wan X-C (2009) A method for determination of imidacloprid residue in tea with HPLC-UV. J Tea Sci 32:203–209
28. Hou X, Yu H, Zhu F, Li Z, Yang Q (2022) Determination of organophosphorus pesticides based on graphene oxide aerogel solid phase extraction column. Chin J Chromatogr 40:10–16
29. Zhao D, Tang H, Wang H, Yang C, Li Y (2020) Analytes triggered conformational switch of i-motif DNA inside gold-decorated solid-state nanopores. ACS Sens 5:2177–2183
30. Siwy Z, Heins E, Harrell CC, Kohli P, Martin CR (2004) Conical-nanotube ion-current rectifiers: the role of surface charge. J Am Chem Soc 35:10850–10851
31. Zhang S, Liu G, Chai H, Zhao Y-D, Yu L, Chen W (2019) Detection of alkaline phosphatase activity with a functionalized nanopipette. Electrochem Commun 99:71–74
32. Xie Z, Yang M, Luo L et al (2020) Nanochannel sensor for sensitive and selective adamantanamine detection based on host-guest competition. Talanta 219:121213
33. Xue L, Yamazaki H, Ren R, Wanunu M, Ivanov AP, Edel JB (2020) Solid-state nanopore sensors. Nat Rev Mater 5:931–951
34. Volcke C, Gandhiraman RP, Gubala V et al (2010) Reactive amine surfaces for biosensor applications, prepared by plasma-enhanced chemical vapour modification of polyolefin materials. Biosens Bioelectron 25:1875–1880
35. Zhang Z, Zhao Q, Yuan J, Antonietti M, Huang F (2014) A hybrid porous material from a pillar[5]arene and a poly(ionic liquid): selective adsorption of n-alkylene diols. Chem Commun 50:2595–2597
36. Kong D, Chen Z (2018) Open-tubular capillary electrochromatography using carboxylatopillar[5]arene as stationary phase. Electrophoresis 39:363–369
37. Siwy ZS (2006) Ion-current rectification in nanopores and nanotubes with broken symmetry. Adv Funct Mater 16:735–746
38. Wang L, Ma Y, Wang L (2021) High selectivity sensing of bovine serum albumin: The combination of glass nanopore and molecularly imprinted technology. Biosens Bioelectron 178:113056
39. Perry D, Momotenko D, Lazenby RA, Kang M, Unwin PR (2016) Characterization of Nanopipettes. Anal Chem 88:5523–5530
40. Zhang M, Gong Z, Yang W et al (2020) Regulating host−guest interactions between cucurbit[7]uril and guests on gold surfaces for rational engineering of gold nanoparticles. ACS Appl Nano Mater 3:4283–4291
41. Sun J, Guo F, Shi Q et al (2019) Electrochemical detection of paraquat based on silver nanoparticles/water-soluble pillar[5]arene functionalized graphene oxide modified glassy carbon electrode. Electroanal Chem 847:113221
42. Jafarinejad Sh (2015) Recent advances in determination of herbicide paraquat in environmental waters and its removal from aqueous solutions: a review. Int Res J Appl Basic Sci 9:1758–1774